frontiers | Frontiers in Materials

TYPE Review
PUBLISHED 12 January 2024
DOI 10.3389/fmats.2023.1339386

OPEN ACCESS

EDITED BY
Mijia Yang,
North Dakota State University, United States

REVIEWED BY
Yang Wei,
Nanjing Forestry University, China
Jun-Jie Zeng,
Guangdong University of Technology, China

*CORRESPONDENCE
Shuaiqi Song,
30070507@huuc.edu.cn
Bowen Zhang,
z1303431002@163.com

RECEIVED 16 November 2023
ACCEPTED 27 December 2023
PUBLISHED 12 January 2024

CITATION
Song S, Zhang B, You P and Yang X (2024), A review study on axial compression properties of UHPC columns confined by FRP.
Front. Mater. 10:1339386.
doi: 10.3389/fmats.2023.1339386

A review study on axial compression properties of UHPC columns confined by FRP

Shuaiqi Song[1]*, Bowen Zhang[2]*, Peibo You[1] and Xiaolong Yang[1]

[1]School of Civil and Transportation Engineering, Henan University of Urban Construction, Pingdingshan, China, [2]School of Architectural Engineering, Zhongyuan University of Technology, Zhengzhou, China

The failure of ultra-high performance concrete (UHPC) under axial compression has significant brittleness, so it is necessary to use fiber reinforced polymer (FRP) to constrain UHPC for achieving ductile failure. This article mainly summarized the research progress of FRP constrained UHPC columns, analyzed the influence of different variables on the compressive performance of FRP-confined UHPC columns and the coupling effect between variables, compared the axial compressive stress-strain models of FRP-confined UHPC columns proposed by previous scholars, and evaluated the existing models using a large amount of collected experimental data. The evaluation results indicated that the existing models provided relatively accurate predictions for ultimate stress, but further improvement and correction are needed for predicting ultimate strain. Based on the data collected in this study, the models had been modified, resulting in improved accuracy in predicting both ultimate stress and ultimate strain.

KEYWORDS

FRP, axial compression, constitutive model, UHPC, column

1 Introduction

Ultra-high performance concrete (UHPC) is a novel cement-based composite material with high strength, high toughness and high durability, which is of great significance for reducing structural weight and improving the structural safety and durability. It can be used in bridges, municipal engineering, industrial plants with corrosion, super high-rise buildings and military engineering (Cheng et al., 2021; Ma et al., 2021; Liu et al., 2022; Wang, 2022; Zhang et al., 2023a; Mu et al., 2023). Due to the significant brittleness of UHPC under axial compression, which gives an unexpected failure mode and behavior (Dang et al., 2022). In order to improve the brittleness of UHPC, many scholars have added different fibers to UHPC to improve the toughness of the material. Liao et al. (2023a) found that increasing the straight steel fiber (SF) content from 1% to 2% could result in a 24% enhancement in the punching shear capacity. Yu et al. (2018) incorporated polyethylene (PE) fibers into UHPC, and the results showed that the adoption of PE fibers might benefit the punching shear resistance of UHPC slabs. Xu et al. (2019) studied the strengthening effect of steel-polypropylene hybrid fiber on UHPC. The results showed that steel-polypropylene hybrid fiber was able to better enhance the strength and the ductility of UHPC. Existing studies (Wu et al., 2006; Shan and Zhang, 2019; Alwesabi et al., 2022; Zhang et al., 2023b; Mu et al., 2023) have shown that adding a certain amount of fiber can effectively improve the brittleness of concrete, but the concrete post-peak behavior such as the ductility and toughness are improved finitely.

Circumferential constraints are imposed on the periphery of the UHPC column, so that the core UHPC is in a three-way compression state, which can not only improve the bearing capacity of the UHPC column, but also greatly improve its ductility. At present, the most widely used are steel and fiber reinforced polymer (FRP) (Xu et al., 2019; Zhao et al., 2022a; Zhao et al., 2023a; Zhao et al., 2023b; Miao et al., 2023; Zeng et al., 2023). Fiber reinforced polymer has light weight and high strength, and its thermal expansion coefficient is similar to that of concrete, which can be coordinated with the deformation of concrete. It is widely used in repair and reinforcement engineering (Yağar et al., 2022; Wang et al., 2023a), bridge engineering (Davids et al., 2022; De Corte and Uyttersprot, 2022), marine engineering (Chen et al., 2023; Zeng et al., 2023), geotechnical engineering (Giraldo and Rayhani, 2014; Wang et al., 2018a) and various civil buildings (Tbatou and El Youbi, 2020). Lateral confinement of UHPC with FRP can give full play to the advantages of UHPC and FRP, and improve the strength and deformation capacity of core UHPC (Liang et al., 2020).

This paper mainly introduced the research progress of axial compression performance of FRP-confined UHPC columns, and described the failure modes of FRP-confined UHPC columns under axial compression. Furthermore, the effects of different parameters and their coupling effects on the axial compression performance of FRP-confined UHPC columns were summarized. Finally, a database was established by analyzing the collected experimental data, the utilization effects of FRP-confined UHPC column constitutive models proposed by previous scholars were compared and evaluated. Based on the established database, the modified model of the existing constitutive models was proposed.

2 Experimental phenomenon of compression of UHPC columns confined by FRP

2.1 Failure modes

The failure modes of FRP-confined UHPC columns under axial compression are closely related to the confinement levels and steel fiber content. Previous studies have shown (Guler, 2014; Wang et al., 2018b; Liang et al., 2020; Lam et al., 2021; Liao et al., 2021; Dang et al., 2022) that FRP has no constraint effect on specimens at the initial stage of loading. With the increase of load, UHPC begins to expand, which leads to the binding effect of FRP on UHPC. As the load continues to increase, the sound of FRP rupture can be heard (Ma et al., 2022). Until the load reaches 90% of the ultimate strength, the middle part of the FRP breaks horizontally and separates from the UHPC column. At this time, the surface of the UHPC column produces longitudinal shear cracks and penetrates into the entire specimen. Longitudinal shear cracks are generated on the UHPC column surface and penetrate through the entire specimen. Due to the bridging effect of steel fiber, the surface crack of UHPC is effectively suppressed. With the increase of steel fiber content, the bearing capacity of the sample increases, and the energy release at the time of failure also increases, which leads to a wider range of FRP fracture and a louder explosion sound. When the lateral restraint stiffness is insufficient, the shear fracture surface is prone to occur under shear stress. The final failure mode of the sample is typical shear failure, and the fracture of FRP is located near the end of the sample. With the increase of confining stiffness, FRP can provide enough lateral confinement, resulting in the emergence of more shear failure planes on UHPC cylindrical specimens under tri-axial compression. The fracture of FRP usually occurs at the middle height of the specimen. The axial compressive failure modes of two different types of FRP-confined specimens under different confinement strengths are shown in Figures 1, 2.

2.2 Stress-strain relationship

Different from the stress-strain relationship of the bilinear behavior of FRP-constrained normal strength concrete (Lam and Teng, 2003), the stress-strain relationship of FRP-constrained UHPC is similar to that of FRP-constrained high strength concrete, which usually shows strength loss after the first peak value (Fallah Pour et al., 2019). The axial compression stress-strain curve of FRP-confined UHPC can be divided into three stages: linear elastic section, transition section and strengthening section. In the transition section, there are two trends with different constraint strength curves, and the typical stress–strain behaviors are shown in Figure 3.

(i) Linear elastic section. In the early loading phase, the FRP constraint is not activated, and its axial stress-strain relationship is similar to that of unconstrained UHPC (Luo et al., 2020).

(ii) Transition section. With the increase of load, micro cracks begin to appear within UHPC, and the confinement effect of FRP is activated with the expansion of core concrete. In case of sufficient circumferential constraint, the axial stress of the specimen will increase with the increase of axial deformation. In case of insufficient circumferential constraint, the load drops sharply due to the brittleness of UHPC, which results a rapid expansion of longitudinal cracks. Meanwhile, the stress-strain curve shows a strength loss after the first peak.

(iii) Strengthening section. At this stage, as the FRP confinement is fully activated, the stress-strain curve enters the second linear rising stage. The slope of the stress-strain curve depends on the confinement efficiency in this stage.

A large number of these studies (Saleem et al., 2017; Zeng et al., 2020; Liao et al., 2021; Wang et al., 2021) have shown an axial stress–strain response different from the typical “bi-linear” curve which ascends monotonically without stress reduction. Instead, strain softening behavior (i.e., stress reduction) has been frequently reported after the curve exceeds the initial peak point, in most cases the stress reduction is followed by a strain hardening response (i.e., stress recovery). In view of the strength loss, it may have an adverse effect on the performance of the column (such as excessive deformation or instability). Therefore, many scholars have studied the stress reduction-recovery behavior of FRP-confined UHPC short columns. Yuan et al. (2022a) showed that the factors leading to the stress-strain softening curve of FRP confined concrete

FIGURE 1
Carbon FRP constrained specimen failure morphology (Liao et al., 2021).

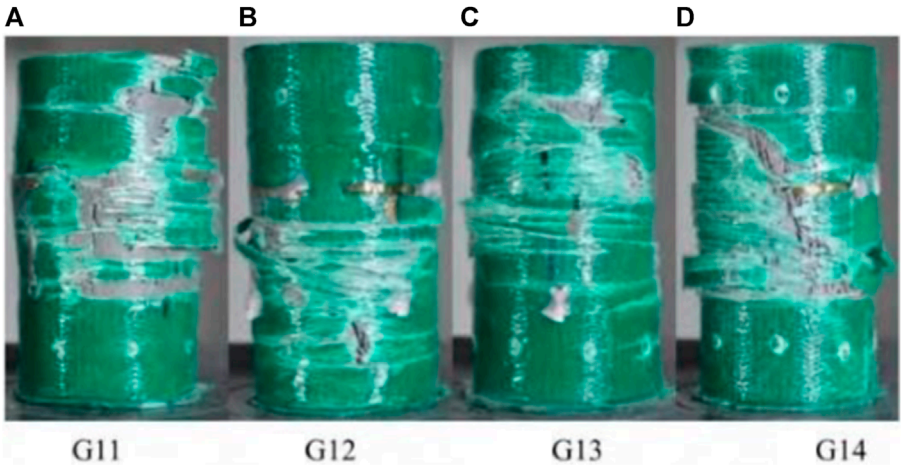

FIGURE 2
Glass FRP constrained specimen failure morphology (Ma et al., 2022). **(A)** G11, **(B)** G12, **(C)** G13, **(D)** G14.

include constraint stiffness, section type and concrete strength. Wu et al. (2006) studied the conditions and reasons for the softening section of the stress-strain curve of FRP confined concrete. The results showed that the softening section of the stress-strain curve of the confined specimen was mainly related to the lateral restraint strength f_1/f'_{co}. When the f_1/f'_{co} of FRP-confined concrete was greater than 0.13, the stress-strain curve had no softening section, otherwise, the stress-strain curve had a softening section. Liao et al. (2023b) explored the root cause of the axial compression stress reduction-recovery behavior of FRP-confined concrete short columns, and determined the five root causes of stress reduction: 1) concrete core brittleness; 2) concrete core shrinkage; 3) non-uniform confinement due to the column shape; 4) insufficient confinement due to the characteristics of FRP materials or fiber orientations; and 5) the arching action. For the remedies, increasing FRP confinement level appears to be a uniform technique except for concrete core shrinkage, whereas increasing steel fiber content and corner radius ratio are more efficient for specimens with brittle concrete cores and specimens in square and rectangular columns, respectively.

3 Analysis of influencing factors on compression properties of FRP-confined UHPC columns

3.1 Steel fiber content

Steel fibers introduced in UHPC column can improve the toughness of UHPC material, while steel fiber is one of the important reasons for the high cost of UHPC. Hence, optimizing the content of steel fiber is of great significance for promoting UHPC (Zhao et al.,

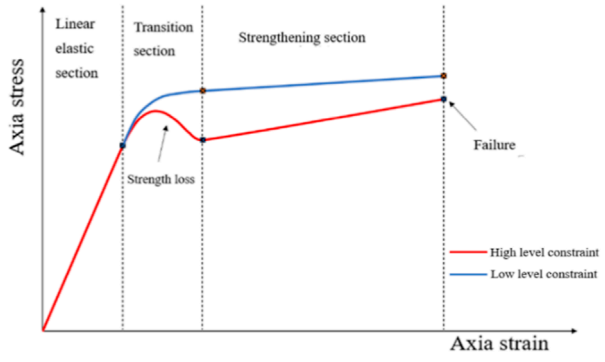

FIGURE 3
Stress-strain curve of FRP-confined UHPC strain hardening.

2022b). Previous studies (Yoo et al., 2013; Hannawi et al., 2016; Wu et al., 2016; Chen et al., 2024) had found that the initial elastic modulus and compressive strength of unconstrained UHPC can be improved with the addition of steel fiber within the appropriate dosage range. However, when the dosage exceeds the limit, the fluidity and mechanical properties of UHPC tend to decrease. Although the toughness of UHPC can also be improved by adding steel fibers, the improvement effect is limited that the ultimate load-bearing capacity of UHPC members cannot be greatly enhanced in practical engineering (Hoang et al., 2019). Therefore, many scholars began to pay attention to improving the ultimate bearing capacity of UHPC by confining it with FRP. Wang et al. (Wang et al., 2018b) carried out an axial compression test on FRP-confined UHPC, and the results showed that steel fiber could effectively inhibit crack expansion and spalling of concrete. Liao et al. (2021) showed that the addition of steel fiber improved the compressive strength of UHPC, and slightly increased the axial strain corresponding to the compressive strength. Tian et al. (2020) established a finite element model of LS-DYNA and analyzed the effect of steel fiber content on the axial compressive properties of constrained specimens. The results showed that increasing the steel fiber content could limit the development of inclined cracks in core UHPC, but it had little effect on the strength and ductility of the specimens. Liang et al. (2020) studied the influence of steel fiber content on the axial compressive properties of UHPC specimens confined by FRP. The results showed that the strength and toughness of FRP-confined UHPC specimens could be improved by adding proper amount of steel fiber. Ma et al. (2022) studied the axial compression properties of FRP-confined UHPC short columns, and the results showed that steel fiber could improve the brittleness characteristics of FRP-confined UHPC short columns to some extent. The existing literature mostly focuses on the study of single steel fiber content, and lacks the study of steel fiber shape, arrangement and hybrid fiber.

3.2 FRP types

In recent years, the use of FRP composites has greatly increased, among which carbon, glass and aramid fibers are the most popular. Guler, (2014) studied the axial compression properties of UHPC short columns wrapped with carbon FRP (CFRP), glass FRP (GFRP) and aramid FRP (AFRP) respectively. The ultimate strength of UHPC columns wrapped with CFRP increased the most, with an increase of 48%, and that of UHPC columns wrapped with GFRP and AFRP increased by 16.8% and 22.7% respectively. The ultimate strain of UHPC columns wrapped by GFRP increases the most, with an increase of 128%, while the ultimate stress of UHPC columns wrapped by AFRP and CFRP increases by 96.9% and 88.9% respectively. Deng, (2016); Deng and Liu, (2016) conducted axial compression tests on UHPC columns constrained by four different fibers: CFRP, GFRP, AFRP and basalt FRP. The results showed that CFRP had the most obvious effect on improving compressive strength, and GFRP had the most obvious effect on improving ultimate strain. Through a large number of studies, it was found that CFRP and GFRP could improve the axial compression performance of constrained specimens more significantly. Therefore, more and more scholars had carried out research on those two fiber materials. Wang et al. (2018b) believed that GFRP had higher tensile strain capacity than CFRP, so it was more suitable to provide constraints for UHPC. An et al. (2021)), Dang et al. (2022), Ma et al. (2022) compared the two fiber types of CFRP and GFRP. The results showed that CFRP could better improve the ultimate strength of short concrete columns than GFRP, and the number of CFRP layers required for strain hardening phenomenon was less than that of GFRP. Compared with CFRP confined specimens, the transverse strain distribution of GFRP confined specimens was more uniform and the stress redistribution was easier. When the number of FRP layers and the volume of steel fiber were unchanged, the strengthening effect of CFRP on the ultimate strength of circular short columns was obviously better than that of GFRP.

3.3 FRP thickness

Deng and Liu, (2016) thought that the ultimate strength and ultimate strain of confined specimens were related to the confined ratio of specimens. Therefore, the thickness of FRP was the key factor affecting the axial compression performance of specimens. Tian et al. (2019a); Tian et al. (2020) studied the axial compression performance of constrained samples with varying FRP tube thickness. The results showed that the deformation of FRP-confined UHPC specimens with small tube thickness went through three stages: linear elasticity, softening and linear strengthening. However, when the tube thickness was increased to provide sufficient constraints, the deformation of the specimen would directly transition from linear elastic stage to linear strengthening stage. Liang et al. (2020) analyzed the influence of GFRP tube thickness on the axial compression performance of the specimens. The results showed that the thicker the tube, the greater the increase in the ultimate strength, and showed a linear growth relationship. Liao et al. (2021) had studied the influence of the number of CFRP layers on the stress-strain curve. The results showed that the FRP thickness mainly affected the transition section and the strengthening section of the curve. In addition, the increased FRP thickness could also alleviate the sudden stress reduction at the first peak, or even eliminate the stress reduction. Ma et al. (2022),

TABLE 1 Summary of existing models.

Model	Ultimate strength (f'_{cf})	Ultimate strain (ε_{cf})
Teng et al. (2009)	$\frac{f'_{cf}}{f'_{co}} = 1+3.5\,(\rho_k - 0.001),\ \rho_\varepsilon\rho_k \geq 0.001$	$\frac{\varepsilon_{cf}}{\varepsilon_{co}} = 1.75 + 6.5{\rho_k}^{0.8}{\rho_\varepsilon}^{1.5},\quad \rho_k = \frac{2E_f t_f}{(f'_{co}/\varepsilon_{co})D},\quad \rho_\varepsilon = \frac{\varepsilon_{h,rup}}{\varepsilon_{co}}$
Cui and Sheikh (2010)	$\frac{f'_{cf}}{f'_{co}} = \left(1 + 10\frac{f_{l,a}}{f'_{co}}\right)^{0.6}$	$\frac{\varepsilon_{cf}}{\varepsilon_{co}} = 1 + [70 - 13\ln(f'_{co})]\left(\frac{f_{l,a}}{f'_{co}}\right)$
Zohrevand and Mirmiran (2013)	$\frac{f'_{cf}}{f'_{co}} = 1 + 3.2519\frac{f_{l,a}}{f'_{co}}$	$\frac{\varepsilon_{cf}}{\varepsilon_{co}} = 1.1075 + 8.836\left(\frac{E_f t_f}{E_c D}\right)\left(\frac{\varepsilon_{h,rup}}{\varepsilon_{co}}\right)^2$
Guler (2014)	$\frac{f'_{cf}}{f'_{co}} = 1 + 0.55\frac{f_{l,a}}{f'_{co}}$	
Deng and Wang (2015)	$\frac{f'_{cf}}{f'_{co}} = 1 + 2.11\left(\frac{f_{l,a}}{f'_{co}}\right)^{1.01}$	$\frac{\varepsilon_{cf}}{\varepsilon_{co}} = 1.65 + 3.95\frac{E_f t}{E_{seco}R}\left(\frac{\varepsilon_f}{\varepsilon_{co}}\right)^{1.32}$
Liang et al. (2020)	$\frac{f'_{cf}}{f'_{co}} = 1 + 2.14\frac{f_{l,a}}{f'_{co}}$	$\frac{\varepsilon_{cf}}{\varepsilon_{co}} = 1 + 5\frac{E_f t}{E_{seco}R}\left(\frac{\varepsilon_f}{\varepsilon_{co}}\right)^{1.58}$
Dang et al. (2022)	$\frac{f'_{cf}}{f'_{co}} = 1 + 3.38\frac{f_{l,a}}{f'_{co}} = 1 + 3.38\rho_k\rho_\varepsilon$	$\frac{\varepsilon_{cf}}{\varepsilon_{co}} = 1 + 17.4{\rho_k}^{0.9}{\rho_\varepsilon}^{0.73}$
Liao et al. (2022)	I: $\frac{f'_{cf}}{f'_{co}} = 0.56 + 2.35\left(\frac{f_{l,a}}{f'_{co}}\right)^{0.6}\left(\frac{\varepsilon_{h,rup}}{\varepsilon_{co}}\right)^{0.1}$	$\frac{\varepsilon_{cf}}{\varepsilon_{co}} = 1.263 + 1.809\left(\frac{f_{l,a}}{f'_{co}}\right)^{0.1}\left(\frac{\varepsilon_{h,rup}}{\varepsilon_{co}}\right)^{0.7}$
	II: $\frac{f'_{cf}}{f'_{co}} = 1 + 0.606\left(\frac{f_{l,a}}{f'_{co}}\right)^{0.6}\left(\frac{\varepsilon_{h,rup}}{\varepsilon_{co}}\right)^{0.7}$	$\frac{\varepsilon_{cf}}{\varepsilon_{co}} = 1 + 0.595\left(\frac{f_{l,a}}{f'_{co}}\right)^{0.1}\left(\frac{\varepsilon_{h,rup}}{\varepsilon_{co}}\right)^{1.45}$

Note: f'_{co}—unconfined compressive strength of UHPC; ε_{co}—axial strain corresponding to the unconfined strength of UHPC; f'_{cf} and ε_{cf}—ultimate axial stress at failure of FRP confinement and its corresponding axial strain respectively; ρ_k—the confinement stiffness; ρ_ε—the strain ratio; E_f—tensile elastic modulus of FRP; t_f—FRP thickness; D—diameter of the specimen; $\varepsilon_{h,rup}$—hoop rupture strain; $f_{l,a}$—actual ultimate confining pressure; E_c—compressive modulus of the UHPC core; ε_f—the ultimate strain of FRP; E_u—the secant modulus of unconstrained specimen at the peak point; R—the radius of core UHPC.

An et al. (2021), Zohrevand and Mirmiran, (2011) studied the axial compression properties of constrained samples with various FRP layers. The results showed that the ultimate compressive strength and ultimate strain of UHPC circular short columns increased with the increase of FRP layers, but the increase of ultimate strain was more substantial.

3.4 Fiber winding angles

When studying FRP-constrained UHPC short columns, most scholars focus primarily on the types and thicknesses of FRP, with less attention given to the winding angles of the FRP fibers. Zhang et al. (2019) conducted the axial compression tests of GFRP-confined concrete short columns with fiber winding angles of ±45, ±60 and ±80°. The results indicated that the winding angles of fibers had a significant impact on the circumferential stiffness and circumferential failure strain of GFRP pipes. Lu, (2020) studied the influence of GFRP-confined UHPC specimens with two different fiber winding angles (60 and 80°) on their mechanical properties. The results showed that the greater the fiber winding angle, the more significant the improvement of compressive strength of the specimen, but it had little effect on the ultimate strain of the specimen. This is consistent with the research results of FRP-confined normal-strength concrete (NSC) (Sadeghian et al., 2010; Vincent and Ozbakkaloglu, 2013). Tian et al. (2019b); Tian et al. (2020) established a micro-finite element model of FRP-confined UHPC cylinder using LS-DYNA finite element analysis software, and studied the influence of fiber winding angles on constrained specimens. The results showed that the ultimate bearing capacity and ductility of specimens increased with the increase of fiber winding angles. Zhu et al. (2023) studied the axial compressive properties of GFRP-confined UHPC with two different fiber winding angles of 45 and 80°. The results showed that, when the axial compression ratio was constant, the ultimate horizontal bearing capacity and equivalent stiffness of the 45° winding tubular composite columns were lower than those of the 80° winding tubular composite columns. However, the former had higher ductility coefficient, better energy dissipation capacity and stronger restraint effect of GFRP tube on UHPC. Vincent and Ozbakkaloglu, (2013) investigated HSC cylinders confined with 3-ply AFRP with different winding angles (i.e., 45°, 60°, 75° and 88°). The results concluded that the confinement effect and ultimate axial stress could decrease when the fiber orientations were further deviated from hoop direction, whereas the ultimate axial strains could increase. Therefore, it is more effective to align the FRP fibers in the hoop direction, which leads to a smaller Poisson's ratio and thus tighter confinement.

From the results in the above literature, it can be concluded that FRP-confined UHPC columns can significantly improve the ultimate strength and strain of axial compression. Different fiber reinforced composites have different reinforcement effects on UHPC. Among them, CFRP has a significant improvement in the ultimate strength of circular short columns, and GFRP has a significant improvement in the ultimate strain of circular short columns. With the increase of FRP thickness, the lateral restraint stress of the specimen increases, which can more effectively restrain the lateral deformation of UHPC in the core area, thus improving the compressive strength and ultimate strain of the specimen. The ultimate strength and ultimate strain of UHPC round short columns can be improved with the increase of the volume of steel fiber, and the brittleness of the specimens can be improved to a certain extent. However, when the volume of steel fiber is too high, the strength of the structure will be adversely affected. From previous studies, it can be inferred that the steel fiber content should not exceed 3%. For FRP-confined UHPC columns, there is a lack of research on the shape and arrangement of steel fibers. With the increase of fiber winding angle, the limit bearing capacity of constrained samples increases, but it has little effect on the ultimate axial strain. At present, the research on the

10.3389/fmats.2023.1339386

TABLE 2 Stress-strain model test database.

Sample number	f'_{cf} (MPa)	ε_{cf}	f'_{co} (MPa)	ε_{co}	$f_{l,a}$ (MPa)	E_f (Gpa)	t_f (mm)	$\varepsilon_{h,rup}$	D (mm)
Liao et al. (2021)									
S100-C1V0-I	115.48	0.0086	127.85	0.00321	8.04	227.3	0.167	0.0106	100
S100-C1V0-II	103.90	0.0112	127.85	0.00321	6.25	227.3	0.167	0.0082	100
S100-C1V1-I	143.27	0.0104	136.33	0.00346	7.63	227.3	0.167	0.01	100
S100-C1V1-II	116.80	0.0125	136.33	0.00346	7.37	227.3	0.167	0.0097	100
S100-C1V2-I	165.44	0.0116	148.9	0.00373	8.27	227.3	0.167	0.0109	100
S100-C1V2-II	181.32	0.009	148.9	0.00373	7.76	227.3	0.167	0.0102	100
S100-C2V0-I	154.85	0.0133	127.85	0.00321	10.08	227.3	0.334	0.0066	100
S100-C2V0-II	157.50	0.0125	127.85	0.00321	12.04	227.3	0.334	0.0079	100
S100-C2V1-I	162.79	0.0146	136.33	0.00346	14.86	227.3	0.334	0.0098	100
S100-C2V1-II	150.55	0.0112	136.33	0.00346	11.82	227.3	0.334	0.0078	100
S100-C2V2-I	215.07	0.0131	148.9	0.00373	12.92	227.3	0.334	0.0085	100
S100-C2V2-II	185.63	0.0162	148.9	0.00373	18.23	227.3	0.334	0.012	100
S100-C3V0-I	192.57	0.0182	127.85	0.00321	13.83	227.3	0.501	0.0061	100
S100-C3V0-II	166.43	0.0119	127.85	0.00321	20.76	227.3	0.501	0.0091	100
S100-C3V1-I	195.55	0.0161	136.33	0.00346	24.36	227.3	0.501	0.0107	100
S100-C3V1-II	202.17	0.0172	136.33	0.00346	26.8	227.3	0.501	0.0118	100
S100-C3V2-I	262.39	0.0218	148.9	0.00373	25.74	227.3	0.501	0.0113	100
S100-C3V2-II	241.54	0.0158	148.9	0.00373	29.31	227.3	0.501	0.0129	100
S100-G6V0-I	189.43	0.0174	127.85	0.00321	15.93	43.3	2.6	0.0074	100
S100-G6V0-II	151.98	0.0146	127.85	0.00321	18.44	43.3	2.6	0.0086	100
S100-G6V1-I	164.90	0.0191	136.33	0.00346	24.53	43.3	2.6	0.0115	100
S100-G6V1-II	192.94	0.0173	136.33	0.00346	32.96	43.3	2.6	0.0154	100
S100-G6V2-I	222.50	0.0145	148.9	0.00373	26.39	43.3	2.6	0.0123	100
S100-G6V2-II	212.43	0.0147	148.9	0.00373	24.03	43.3	2.6	0.0112	100
S100-G8V0-I	212.65	0.0195	127.85	0.00321	26.36	43.3	3.24	0.0094	100
S100-G8V0-II	190.53	0.0195	127.85	0.00321	33.92	43.3	3.24	0.0121	100
S100-G8V1-I	210.46	0.0163	136.33	0.00346	29.2	43.3	3.24	0.0104	100
S100-G8V1-II	222.50	0.0186	136.33	0.00346	38.86	43.3	3.24	0.0138	100
S100-G8V2-I	241.55	0.0227	148.9	0.00373	40.24	43.3	3.24	0.0143	100
S100-G8V2-II	237.17	0.0169	148.9	0.00373	33.14	43.3	3.24	0.0118	100
S50-C1-V0-I	176.17	0.0147	142.3	0.0032	16.96	227.3	0.167	0.0112	50

(Continued on the following page)

TABLE 2 (*Continued*) Stress-strain model test database.

Sample number	f'_{cf} (MPa)	ε_{cf}	f'_{co} (MPa)	ε_{co}	$f_{l,a}$ (MPa)	E_f (Gpa)	t_f (mm)	$\varepsilon_{h,rup}$	D (mm)
S50-C1-V0-II	184.11	0.0141	142.3	0.0032	16.03	227.3	0.167	0.0106	50
S50-C1-V1-I	181.47	0.0164	151.75	0.00356	13.48	227.3	0.167	0.0089	50
S50-C1-V1-II	198.68	0.0148	151.75	0.00356	12.87	227.3	0.167	0.0085	50
S50-C1-V2-I	211.93	0.0075	156.44	0.00373	17.78	227.3	0.167	0.0117	50
S50-C1-V2-II	185.44	0.0117	156.44	0.00373	17.41	227.3	0.167	0.0115	50
S50-C2-V0-I	234.45	0.02	142.3	0.0032	42.51	227.3	0.334	0.014	50
S50-C2-V0-II	255.64	0.0252	142.3	0.0032	39.59	227.3	0.334	0.013	50
S50-C2-V1-I	280.81	0.0229	151.75	0.00356	33.23	227.3	0.334	0.0109	50
S50-C2-V1-II	260.94	0.0171	151.75	0.00356	34.88	227.3	0.334	0.0115	50
S50-C2-V2-I	287.43	0.0221	156.44	0.00373	41.62	227.3	0.334	0.0137	50
S50-C2-V2-II	241.07	0.0169	156.44	0.00373	38.92	227.3	0.334	0.0128	50
S50-G4V0-I	245.04	0.0211	142.3	0.0032	30.4	43.3	1.8	0.0098	50
S50-G4V0-II	262.26	0.0267	142.3	0.0032	36.2	43.3	1.8	0.0116	50
S50-G4V1-I	255.64	0.0229	151.75	0.00356	54.98	43.3	1.8	0.0176	50
S50-G4V1-II	266.24	0.0208	151.75	0.00356	47.21	43.3	1.8	0.0151	50
S50-G4V2-I	262.26	0.0201	156.44	0.00373	54.95	43.3	1.8	0.0176	50
S50-G4V2-II	251.67	0.0176	156.44	0.00373	46.88	43.3	1.8	0.015	50
S50-G6V1-I	316.57	0.03	151.75	0.00356	61.56	43.3	2.47	0.0137	50
S50-G6V1-II	360.28	0.0318	151.75	0.00356	58.08	43.3	2.47	0.0129	50
Wang et al. (2018b)									
UHPFRC-C1-I	125.30	0.0079	135.89	0.00531	2.61	200	0.167	0.0055	150
UHPFRC-C1-II	85.20	0.0092	135.89	0.00531	2.97	200	0.167	0.0055	150
UHPFRC-C2-I	158.20	0.0106	135.89	0.0055	6.86	200	0.334	0.008	150
UHPFRC-C2-II	107.00	0.0124	135.89	0.0055	9.53	200	0.334	0.008	150
UHPFRC-C3-I	173.40	0.0177	135.89	0.0057	14.75	200	0.501	0.0111	150
UHPFRC-C3-II	163.80	0.0175	135.89	0.0057	19.36	200	0.501	0.0111	150
UHPFRC-C5-I	250.70	0.0199	135.89	0.00659	35.08	200	0.835	0.0139	150
UHPFRC-C5-II	244.00	0.0211	135.89	0.00659	35.85	200	0.835	0.0139	150
UHPFRC-G3-I	159.00	0.0196	135.89	0.005444	12.3	100	0.507	0.018	150
UHPFRC-G3-II	136.30	0.0199	135.89	0.005444	11.97	100	0.507	0.018	150
UHPFRC-G5-I	182.50	0.0273	135.89	0.0055	20.28	100	0.845	0.0178	150
UHPFRC-G5-II	171.20	0.0207	135.89	0.0055	19.83	100	0.845	0.0178	150

(Continued on the following page)

10.3389/fmats.2023.1339386

TABLE 2 (*Continued*) Stress-strain model test database.

Sample number	f'_{cf} (MPa)	ε_{cf}	f'_{co} (MPa)	ε_{co}	$f_{l,a}$ (MPa)	E_f (Gpa)	t_f (mm)	$\varepsilon_{h,rup}$	D (mm)
UHPFRC-G9-I	269.10	0.0322	135.89	0.0066	37.52	100	1.521	0.0184	150
UHPFRC-G9-II	250.30	0.0292	135.89	0.0066	37.11	100	1.521	0.0184	150
UHPC-C1-I	100.70	0.0104	87.99	0.004	3.53	200	0.167	0.0068	150
UHPC-C1-II	96.30	0.0097	87.99	0.004	3.38	200	0.167	0.0068	150
UHPC-C3-I	178.70	0.0195	87.99	0.0048	16.44	200	0.501	0.0102	150
UHPC-C3-II	157.00	0.0192	87.99	0.0048	14.75	200	0.501	0.0102	150
UHPC-C5-I	240.00	0.0262	87.99	0.00566	36.87	200	0.835	0.0143	150
UHPC-C5-II	225.40	0.0252	87.99	0.00566	36.11	200	0.835	0.0143	150
UHPC-G5-I	168.30	0.0261	87.99	0.0053	19.6	100	0.845	0.0165	150
UHPC-G5-II	167.60	0.0306	87.99	0.0053	17.46	100	0.845	0.0165	150
Lu (2020)									
G2A80-SV2-I	198.60	0.0144	110.9	0.00355	28.69	44.4	2.01	0.0161	100
G2A80-SV2-II	192.90	0.0141	110.9	0.00355	24.49	44.4	2.01	0.0137	100
G2A80-SV2-III	176.60	0.0143	110.9	0.00355	25.73	44.4	2.01	0.0144	100
G5A80-SV2-I	293.10	0.0218	110.9	0.00355	84	44.4	4.96	0.0191	100
G5A80-SV2-II	299.50	0.0217	110.9	0.00355	87.83	44.4	4.96	0.0199	100
G5A80-SV2-III	288.40	0.021	110.9	0.00355	79.72	44.4	4.96	0.0181	100
G2A60-SV2-I	146.50	0.0155	110.9	0.00355	15.99	21.2	2.05	0.0184	100
G2A60-SV2-II	162.20	0.0151	110.9	0.00355	16.02	21.2	2.05	0.0184	100
G2A60-SV2-III	157.10	0.0151	110.9	0.00355	17.11	21.2	2.05	0.0197	100
G5A60-SV2-I	200.00	0.0183	110.9	0.00355	50.6	21.2	5.48	0.0218	100
G5A60-SV2-II	200.40	0.0182	110.9	0.00355	43.5	21.2	5.48	0.0187	100
G5A60-SV2-III	196.80	0.019	110.9	0.00355	45.24	21.2	5.48	0.0195	100
G2A80-SV2-II(c)	180.00	0.0138	110.9	0.00355	26.47	44.4	2.01	0.0148	100
G2A80-SV2-III(c)	192.00	0.0136	110.9	0.00355	25.4	44.4	2.01	0.0142	100
G5A80-SV2-I(c)	295.50	0.0245	110.9	0.00355	92.79	44.4	4.96	0.0211	100
G5A80-SV2-II(c)	303.60	0.025	110.9	0.00355	96.2	44.4	4.96	0.0218	100
G5A80-SV2-III(c)	295.50	0.0245	110.9	0.00355	91.18	44.4	4.96	0.0207	100
G2A60-SV2-I(c)	151.00	0.0147	110.9	0.00355	17.54	21.2	2.05	0.0202	100
G2A60-SV2-III(c)	143.20	0.0154	110.9	0.00355	16.28	21.2	2.05	0.0187	100
G5A60-SV2-I(c)	204.10	0.0281	110.9	0.00355	59.05	21.2	5.48	0.0254	100
G5A60-SV2-II(c)	201.40	0.0258	110.9	0.00355	56.37	21.2	5.48	0.0243	100

(Continued on the following page)

TABLE 2 (*Continued*) Stress-strain model test database.

Sample number	f'_{cf} (MPa)	ε_{cf}	f'_{co} (MPa)	ε_{co}	$f_{l,a}$ (MPa)	E_f (Gpa)	t_f (mm)	$\varepsilon_{h,rup}$	D (mm)
G5A60-SV2-III(c)	213.00	0.0292	110.9	0.00355	64.79	21.2	5.48	0.0279	100
G2A80-SV0-I	192.90	0.0141	83.6	0.00271	25.21	44.4	2.01	0.0141	100
G2A80-SV0-II	197.80	0.0134	83.6	0.00271	28.27	44.4	2.01	0.0158	100
G2A80-SV0-III	195.00	0.0135	83.6	0.00271	24.26	44.4	2.01	0.0136	100
G5A80-SV0-I	267.50	0.0181	83.6	0.00271	73.62	44.4	4.96	0.0167	100
G5A80-SV0-II	261.90	0.0162	83.6	0.00271	65.98	44.4	4.96	0.015	100
G2A80-HV2-I	194.00	0.0131	115.4	0.00364	26.05	44.4	2.01	0.0146	100
G2A80-HV2-II	202.70	0.0122	115.5	0.00364	27.31	44.4	2.01	0.0153	100
G2A80-HV2-III	205.00	0.0135	115.6	0.00364	30.2	44.4	2.01	0.0169	100
G5A80-HV2-I	298.80	0.0184	115.7	0.00364	70.96	44.4	4.96	0.0161	100
G5A80-HV2-II	296.80	0.0179	115.8	0.00364	70.09	44.4	4.96	0.0159	100
G5A80-HV2-III	304.10	0.0193	115.9	0.00364	72.5	44.4	4.96	0.0165	100
G2A80-SV2(H)-I	171.00	0.0119	131.2	0.00438	24.54	44.3	2.01	0.0138	100
G2A80-SV2(H)-III	178.20	0.0127	131.2	0.00438	27.36	44.3	2.01	0.0154	100
G5A80-SV2(H)-I	289.10	0.0265	131.2	0.00438	109.19	44.3	4.96	0.0248	100
G5A80-SV2(H)-II	302.20	0.024	131.2	0.00438	95.72	44.3	4.96	0.0218	100
G5A80-SV2(H)-III	308.00	0.023	131.2	0.00438	91.72	44.3	4.96	0.0209	100

influence parameters of axial compression performance of FRP confined UHPC short columns is insufficient, such as specimen size, slenderness ratio, steel fiber shape and other parameters. Therefore, it is necessary to carry out relevant tests to verify the influence of these parameters on the axial compression performance of confined specimens.

3.5 Analysis of coupling effect of influencing factors

In many studies, it can be observed that there are often multiple experimental variables, so it is necessary to consider the interaction between variables and the synergistic effects of different variables on experimental results.

Tian et al. (2019a) investigated the coupled effects of FRP thickness and steel fiber content on the ultimate strain and compressive strength of FRP-confined UHPC specimens. The results revealed that the influence of steel fiber content was more obvious in the specimens with thinner walls. When the wall thickness was sufficiently thick, the effect of steel fibers was less significant. Liao et al. (2021) investigated the synergistic effects of specimen dimensions, FRP thickness, and steel fiber content. The results demonstrated that, for larger-sized specimens, increasing the steel fiber content had only a slight enhancement effect on specimen toughness at a relatively low confinement level. However, as the confinement level increased, the strengthening effect of increasing steel fiber content became more pronounced. Conversely, for smaller-sized specimens, the impact of steel fiber content on specimen toughness appeared to be insignificant even at a high confinement level. Yoo et al. (2016) investigated the influence of steel fiber shape on the size effect of specimens. The results indicated that the use of longer steel fibers had a more pronounced mitigating effect on the size effect of the specimens. Ma et al. (2022) studied the effects of steel fiber content, types and layers of FRP on the axial compression properties of constrained specimens. The results showed that CFRP improved the ultimate strength of round short columns significantly better than GFRP when the number of FRP layers or steel fiber content was increased. Wang et al. (2023b) investigated the coupling effect of "dual confinement" of FRP and steel fibers on confined specimens. The results showed that the addition of steel fiber could alleviate the stress reduction effect of UHPC specimens. In the later stage of FRP-confined UHPC loading, the existence of steel fibers had little effect on the FRP constraint effect. Most of the existing studies focus on the influence of a single variable on the axial compression properties of constrained samples, while few studies on the coupling effects of multiple variables. Correspondingly, there is a lack of

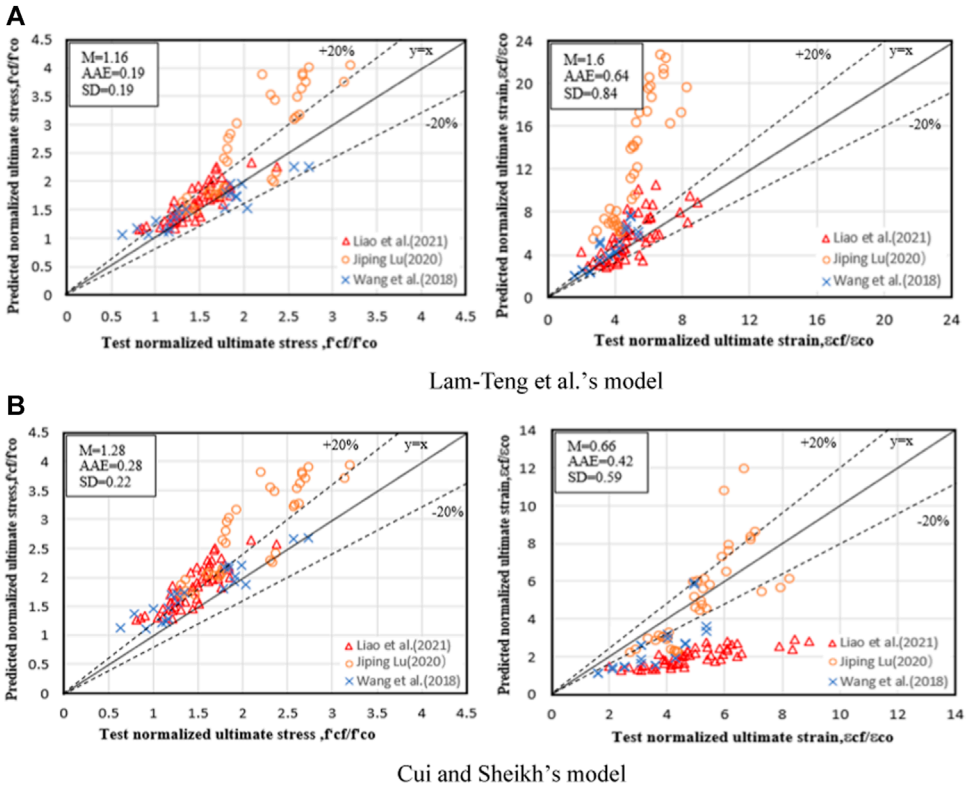

FIGURE 4
(Continued).

comparative analysis of axial compression performance under multiple variables.

4 Constitutive model of FRP-confined UHPC columns under axial compression

4.1 Summary of existing models

Currently, many scholars had conducted numerous experimental studies and theoretical analyses on the axial compression performance and stress-strain relationship of FRP-confined ordinary concrete (Ozbakkaloglu et al., 2013; Deng, 2015; Deng and Qu, 2015; Deng and Wang, 2015; Li and Zhou, 2022). Although some constitutive models had been proposed, most of them were based on the modification of the constitutive model of FRP-confined ordinary concrete to make it suitable for FRP-confined UHPC models.

Zohrevand and Mirmiran, (2011) compared the experimental data with Mander model (Mander et al., 1988), Samaan model (Samaan et al., 1998), Toutanji model (Toutanji, 1999) and Lam-Teng model (Lam and Teng, 2003), respectively. The results showed that the Lam-Teng model provided the best fit for the stress-strain response of most specimens. However, all models tended to underestimate the ultimate strength at higher constraint ratios. None of the models can make reasonable predictions for the ultimate strain of UHPC specimens confined by FRP. Zohrevand and Mirmiran, (2013) modified the stress-strain model of unconfined UHPC proposed by Lam and Teng, and the accuracy of the predicted stress-strain curve was significantly improved. Guler, (2014) proposed a predictive model for FRP-confined UHPC and compared it with a model for FRP-confined conventional concrete. The results showed that the proposed model accurately predicted the ultimate strength, consistent with experimental findings. Deng and Wang, (2015) derived predictive formulas for the ultimate strength and ultimate strain of confined specimens through regression analysis, and modified the intercept in the Lam-Teng model. The modified model was more favorable for predicting the ultimate strength. Liang et al. (2020) conducted axial compression tests on GFRP-confined UHPC specimens and derived formulas to calculate the ultimate compressive strength and ultimate strain of UHPC under GFRP confinement based on experimental results. Wang et al. (2018b) evaluated the existing stress-strain models that can be used for FRP-confined UHPC. The results showed that the strength model proposed by Guler, (2014) provided a better prediction of ultimate strength, and the strain model proposed by Cui and Sheikh, (2010) provided a better prediction of ultimate strain. Liao et al. (2021) evaluated four prediction models and the results showed that the equations proposed by Dang et al. (2022) based on the Lam and Teng, (2003) was more accurate in predicting both ultimate strength and ultimate strain. The above models are shown in Table 1.

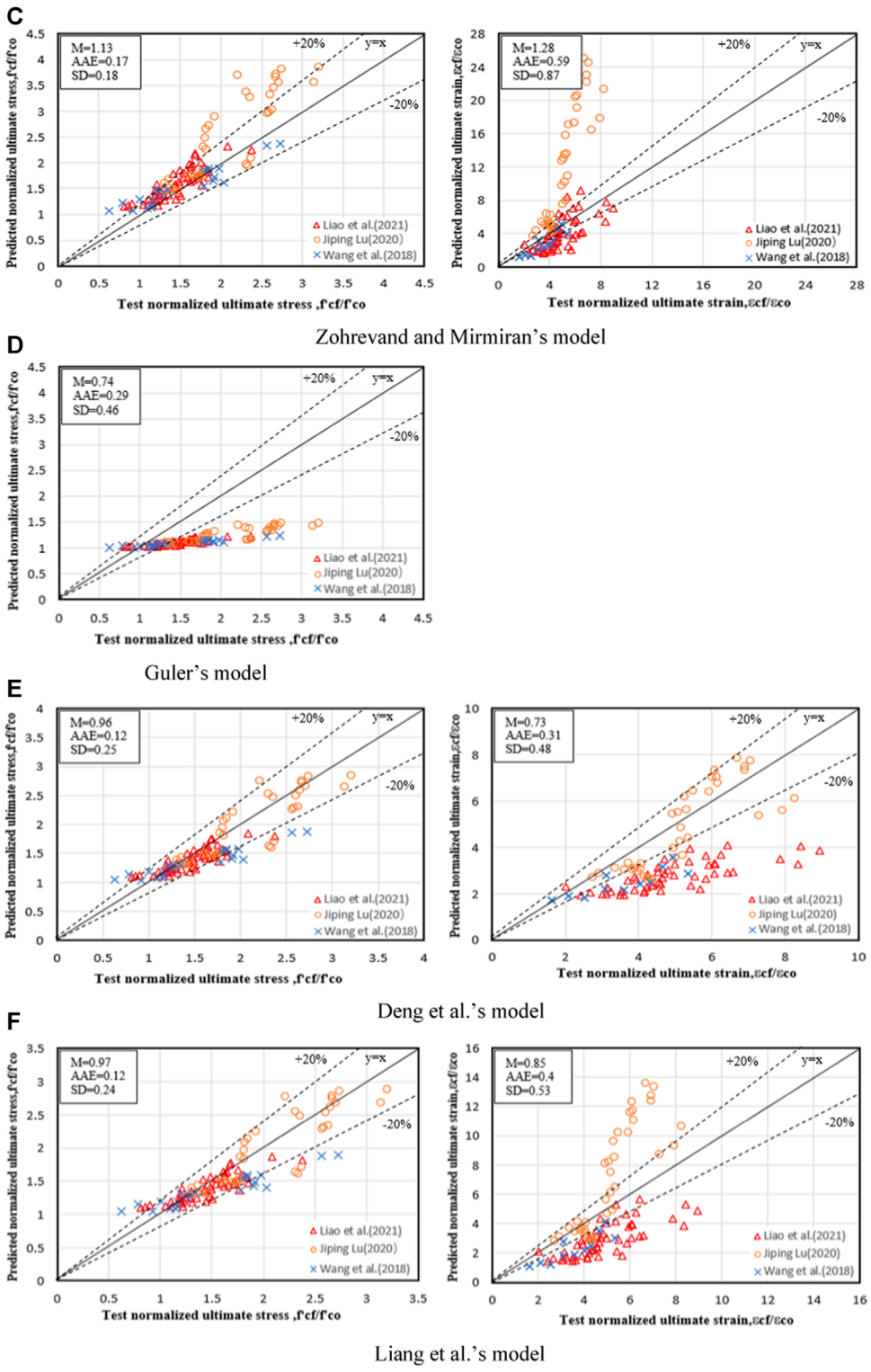

FIGURE 4
(Continued).

4.2 Performance evaluation of existing models

Currently, the understanding of the confinement mechanism of FRP-confined UHPC short columns is relatively mature. Many scholars had conducted a large number of experimental studies and proposed many models. For the axial stress-strain models summarized in the above section, their accuracy needs to be considered. In this section, the above-mentioned models will be evaluated through collected experimental data. To ensure a more

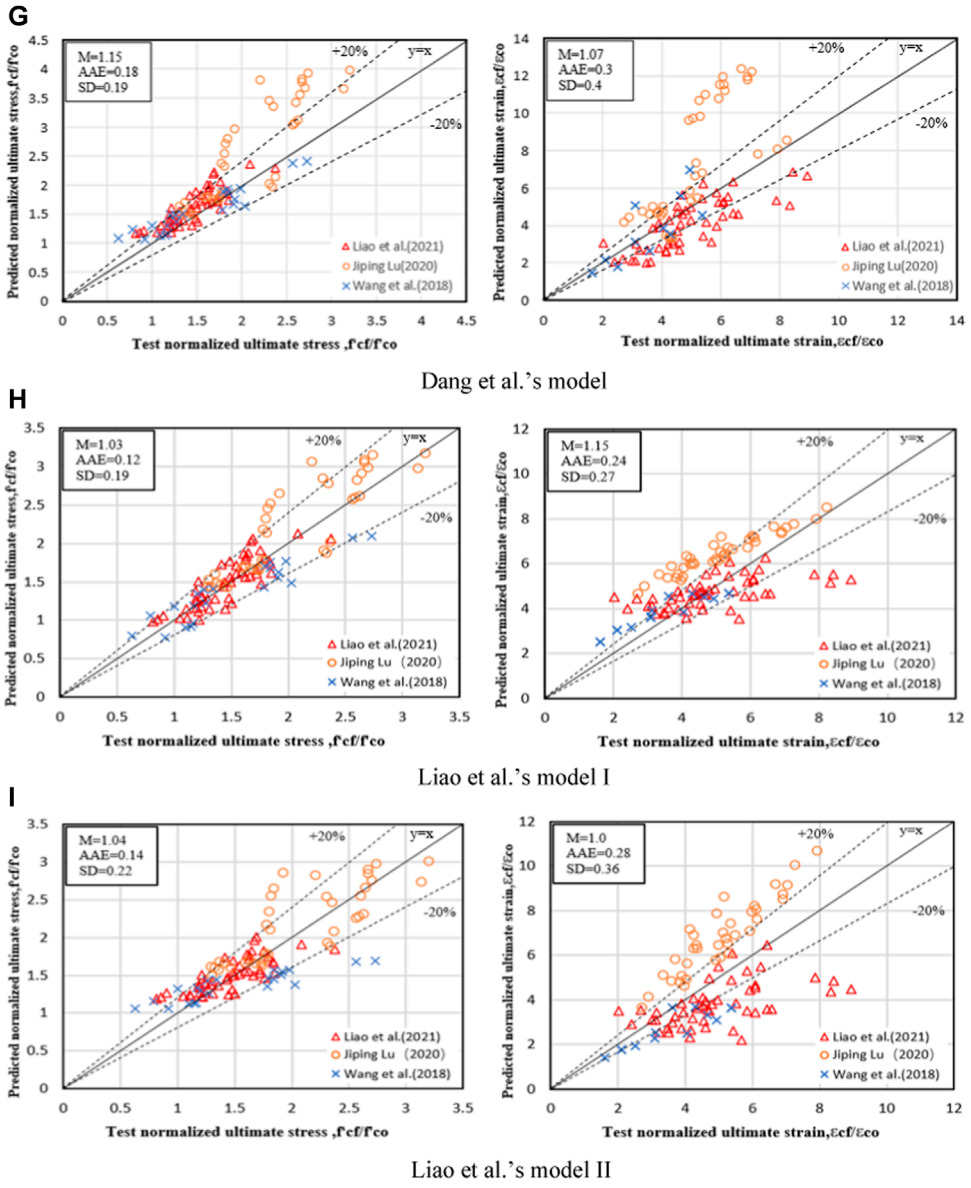

FIGURE 4
(Continued). Comparisons between model predictions and test results. **(A)** Lam Teng model, **(B)** Cui and Sheikh's model, **(C)** Zohrevand and Mirmiran's model, **(D)** Guler's model, **(E)** Deng et al.'s model, **(F)** Liang et al.'s model, **(G)** Dang et al.'s model, **(H)** Liao et al.'s model I, **(I)** L iao et al.'s model II.

reliable evaluation, this study selected experimental data from Liao et al. (2021), Lu, (2020) and Wang et al. (2018b) to establish a fitting sample database, which is listed in Table 2.

In this study, the performance of the above stress-strain models was evaluated and the key results predicted by the above models (normalized ultimate axial stress f'_{cf}/f'_{co}) and normalized ultimate axial strain $\varepsilon_{cf}/\varepsilon_{co}$) were compared with the experimental results. The performance of the selected models was quantified by three statistical indicators: the mean M), the standard deviation (SD), and the average absolute error (AAE) between the test results and the predictions. The M and AAE given by Eqs 1, 2, respectively, were used to evaluate the accuracy of the models, whereas the SD in Eq. 3 quantifies the scattering of predictions from each model. The results of these three indicators are indicated in the comparison chart.

$$M = \frac{\sum_{i=1}^{n} \frac{pred_i}{exp_i}}{n} \tag{1}$$

$$AAE = \frac{\sum_{i=1}^{n} \left| \frac{exp_i - pred_i}{exp_i} \right|}{n} \tag{2}$$

$$SD = \frac{\sum_{i=1}^{n} \left[\frac{pred_i}{exp_i} - \left(\frac{pred}{exp} \right)_{aver} \right]^2}{n-1} \tag{3}$$

where exp_i is the ith experimental result; $pred_i$ is the ith model prediction; and n is the total sample number in the database.

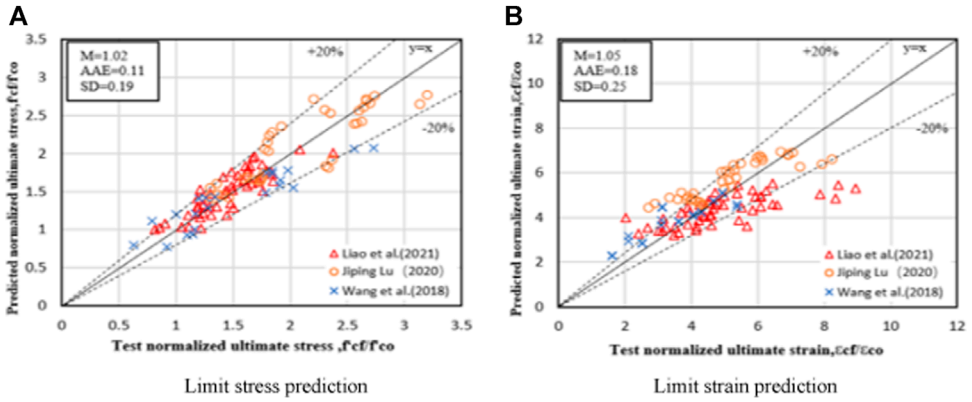

FIGURE 5
Modified model performance. **(A)** Limit stress prediction, **(B)** Limit strain prediction.

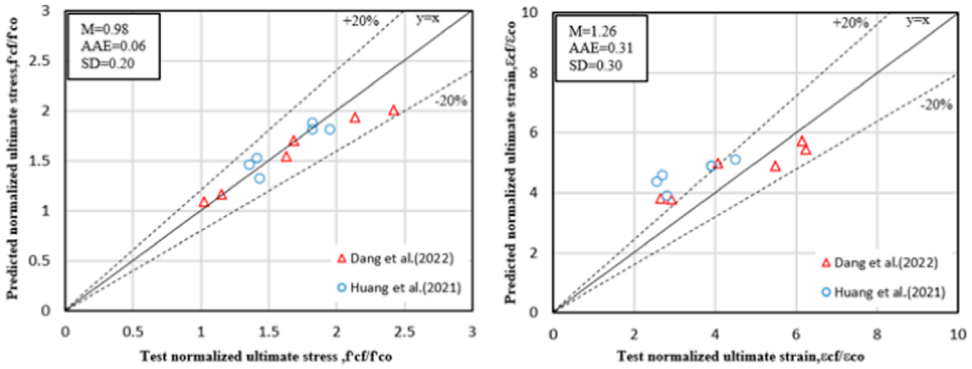

FIGURE 6
Model validation results.

The performance of the selected models is shown in Figure 4. In general, the applicability and accuracy of the selected models are limited. These models can give relatively accurate predictions for the test results of some studies, but cannot provide satisfactory predictions for most test results in the database. It can be observed from Figure 4 that the fitting effect of each model on the test data of Lu, (2020) is poor, mainly due to significant differences in the FRP and UHPC material properties compared to other specimens. For the two models proposed by Liao et al. (2022), they are evaluated only based on the prediction accuracy of ultimate stress and ultimate strain. It is worth noting that the two models proposed by Liao et al. (2022) are suitable for different situations. Because the data of different studies are difficult to coordinate, the accuracy of prediction is affected.

Model I proposed by Liao et al. (2022) is considered as the best model for estimating f'_{cf}/f'_{co}, with high fitting accuracy and low dispersion., and its AAE and SD are 12% and 19%, respectively. The second are the model modified by Liang et al. (2020) and Deng and Wang, (2015). Their AAE are both 12%, but the degree of dispersion is higher than that of Liao et al. (2022), and their SD are 24% and 25% respectively. As can be seen from the comparison of specific test data in Figure 4, both Teng et al. (2009) and Cui and Sheikh, (2010) model tend to overestimate f'_{cf}/f'_{co}, while Guler, (2014) model seriously underestimates f'_{cf}/f'_{co}, resulting in 29% AAE and 46% SD. From the distribution of scatter plots, the test data with higher constraint strength tend to overestimate the test results by about 2–4 times.

The above models have poor performance in estimating extreme strain, among which the model of Liao et al. (2022) has a relatively good estimation of extreme strain, but its AAE is also as high as 24%, and its predictions are relatively discrete. The Teng et al. (2009) model and the modified Lam-Teng model by Zohrevand and Mirmiran, (2013) fit well with the experimental data of Wang et al. (2018b) and Liao et al. (2021), but the predicted results for the test data of Lu (2020) are not satisfactory. The predictions of other models for ultimate strain can only be adapted to their own test results, and cannot provide satisfactory predictions for the majority of test results from other studies.

4.3 Forecasting model modification

Most of the existing prediction models are based on FRP-confined ordinary concrete, and it is believed that the strength

confinement efficiency increases with the increase of confinement ratio. Samaan model (Samaan et al., 1998) believed that the relationship between strength and constraint ratio was nonlinear. Deng and Wang, (2015) modified Samaan model and the predicted value was relatively close to the experimental value. Considering the influence of FRP ultimate strain and constraint stiffness, an empirical formula for predicting the compressive strength of FRP-confined UHPC was obtained by regression of the experimental data collected in this study:

$$\frac{f'_{cf}}{f'_{co}} = 0.35 + 2.566\left(\frac{f_{l,a}}{f'_{co}}\right)^{0.455} \tag{4}$$

Using the regression formula (Eq. 4) for calculations, the predicted values show a good agreement with the experimental values.

On the basis of Zeng et al.'s FRP confined concrete model (Zeng et al., 2020) with the large rupture strain (LRS), Liao et al. obtained the ultimate strain prediction model by regression, and the prediction effect is relatively good. Based on the modified model of Liao et al., the following ultimate strain formula (Eq. 5) was fitted according to the test data collected in this paper, and it exhibits a good predictive performance:

$$\frac{\varepsilon_{cf}}{\varepsilon_{co}} = 5.264\left(\frac{f_{l,a}}{f'_{co}}\right)^{0.216}\left(\frac{\varepsilon_{h,rup}}{\varepsilon_{co}}\right)^{0.168} \tag{5}$$

The fitting effect of the revised model was shown in Figure 5. Compared with the model before correction, the prediction accuracy of the revised model has improved both in terms of ultimate stress and ultimate strain. Especially for the prediction of ultimate strain, the mean value is 1.05, with the AAE reduced to 18%, and the degree of dispersion is also improved. However, the prediction results for ultimate stress and ultimate strain are larger than the experimental values.

In order to verify the reliability and applicability of the modified models, the test data of Huang et al. (2021) and Dang et al. (2022) were selected for simulation. The selected test data are based on the axial compression test of FRP-confined UHPC circular short columns. The models verification results are shown in Figure 6. The prediction accuracy of the ultimate stress is high, and its AAE is 6%, indicating that the modified ultimate stress prediction model has good universality. However, the prediction effect of ultimate strain is far less than that of ultimate stress. Similar trends have also been reported in previous studies on FRP-confined NSC Bai et al. (2019); Pimanmas and Saleem, (2019); Yuan et al. (2022b). First, the stress measurement technique is more reliable than the strain measurement technique, and the strain measurement may be affected by the premature failure of the sample. Secondly, different mix proportions of UHPC and different methods of applying FRP constraints (FRP cloth or tube) may also interfere with the strain measurement results.

5 Conclusion and prospect

Through the study of axial compression test of FRP-confined UHPC short columns and the analysis of its stress-strain relationship models, it can be seen that:

(1) With the increase of FRP thickness, the bearing capacity and ductility of the specimens are improved. Steel fiber can improve the brittle characteristics of UHPC columns, and an appropriate amount of steel fiber can also improve the ultimate bearing capacity of the specimens. With the increase of the fiber winding angles, the ultimate bearing capacity of the confined specimens increases, but it has little effect on the ultimate axial strain. Most of the existing studies focus on a single variable, and there is a lack of research on the coupling effect of multiple variables.

(2) Evaluation of existing models suggests that the modified models by Liang et al. and Deng et al. provide the best predictions with high accuracy for ultimate stress, although the existing models show a good prediction performance for ultimate stress, the prediction of ultimate strain remains unsatisfactory.

(3) Based on the data collected in this study, the axial compression stress-strain model was modified. The modified model has improved the prediction accuracy of both ultimate stress and ultimate strain. Research on the axial stress-strain model of FRP-confined UHPC columns is limited, and further experimental research is needed to refine and validate the existing models.

Author contributions

SS: Supervision, Writing–review and editing. BZ: Writing–original draft. PY: Writing–review and editing. XY: Writing–review and editing.

Funding

The author(s) declare financial support was received for the research, authorship, and/or publication of this article. Financial supports to complete this research were provided partially by the Higher Education Youth Key Teacher Training Program Project (No. 2021GGJS142) of Henan Province and the National Natural Science Foundation Youth Fund Project(No.52108207) of China, both at Henan University of Urban Construction, P. R. China.

Conflict of interest

The authors declare that the research was conducted in the absence of any commercial or financial relationships that could be construed as a potential conflict of interest.

Publisher's note

References

Alwesabi, E. A. H., Abu Bakar, B. H., Alshaikh, I. M. H., Abadel, A. A., Alghamdi, H., and Wasim, M. (2022). An experimental study of compressive toughness of Steel–Polypropylene hybrid Fibre-Reinforced concrete. *Struct.* 37, 379–388. doi:10.1016/j.istruc.2022.01.025

An, K. X., Wang, X. Y., and Liu, Z. X. (2021). Study on axial compression performance research on UHPC short columns confined by fiber reinforced polymer. *Build. Struct.* 51 (11), 129–135. doi:10.19701/j.jzjg.2021.11.021

Bai, Y.-L., Dai, J.-G., Mohammadi, M., Lin, G., and Mei, S. J. (2019). Stiffness-based design-oriented compressive stress-strain model for large-rupture-strain (LRS) FRP-confined concrete. *Compos. Struct.* 223, 110953. doi:10.1016/j.compstruct.2019.110953

Chen, C. C., Wu, Z. M., and Hu, X. (2024). Influence of steel fiber shape and curing system on strength and toughness of UHPC. *Mater. Rep.* 38 (15), 23030088. doi:10.11896/cldb.23030088

Chen, Y., Hu, Y., and Wu, Z. M. (2023). Review on the deterioration of FRP reinforced concrete structures subjected to marine environment. *Mater. Rep.* 37 (18), 83–93. doi:10.11896/cldb.21120052

Cheng, Z., Zhang, Q., Bao, Y., Deng, P., Wei, C., and Li, M. (2021). Flexural behavior of corrugated steel-UHPC composite bridge decks. . *Eng. Struct.* 246, 113066. doi:10.1016/j.engstruct.2021.113066

Cui, C., and Sheikh, S. A. (2010). Analytical model for circular normal- and high-strength concrete columns confined with FRP. *J. Compos. Constr.* 14 (5), 562–572. doi:10.1061/(asce)cc.1943-5614.0000115

Dang, Z., Li, Z., and Feng, P. (2022). Axial compressive behavior of UHPC confined by FRP. *Compos. Struct.* 300, 116110. doi:10.1016/j.compstruct.2022.116110

Davids, W. G., Guzzi, D., and Schanck, A. P. (2022). Development and experimental assessment of friction-type shear connectors for FRP bridge girders with composite concrete decks. *Decks. Mater.* 15 (9), 3014. doi:10.3390/ma15093014

De Corte, W., and Uyttersprot, J. (2022). FRP bridges in the flanders region: experiences from the C-bridge Project. *Appl. Sci.* 12 (21), 10897. doi:10.3390/app122110897

Deng, Z., and Qu, J. (2015). The experimental studies on behavior of ultrahigh-performance concrete confined by hybrid fiber-reinforced polymer tubes. *Adv. Mater. Sci. Eng.* 2015, 1–18. doi:10.1155/2015/201289

Deng, Z. C. (2015). Progress in studies of the constitutive model of FRP-confined concrete columns. *Mech. Eng.* 37 (1), 33–39. doi:10.6052/1000-0879-14-131

Deng, Z. C. (2016). Effects of thicknesses and types of fiber reinforced polymer tubes on theuniaxial compressive behaviors of confined UHPC specimen. *J. Harbin Eng. Univ.* 37 (2), 218–222. doi:10.11990/jheu.201409037

Deng, Z. C., and Liu, S. X. (2016). Test and modeling of ultra-high performance concrete confined by fiber reinforced polymer tube. *J. Basic Sci. Eng.* 24 (4), 792–803. doi:10.16058/j.issn.1005-0930.2016.04.015

Deng, Z. C., and Wang, Y. C. (2015). Axial compression stress-strain model for UHPC cylinders confined by FRP. *J. Southwest Jiaot. Univ.* 50 (4), 641–647. doi:10.3969/j.issn.0258-2724.2015.04.011

Fallah Pour, A., Gholampour, A., Zheng, J., and Ozbakkaloglu, T. (2019). Behavior of FRP-confined high-strength concrete under eccentric compression: tests on concrete-filled FRP tube columns. *Compos. Struct.* 220, 261–272. doi:10.1016/j.compstruct.2019.03.031

Giraldo, J., and Rayhani, M. T. (2014). Load transfer of hollow Fiber-Reinforced Polymer (FRP) piles in soft clay. *Transp. Geotech.* 1 (2), 63–73. doi:10.1016/j.trgeo.2014.03.002

Guler, S. (2014). Axial behavior of FRP-wrapped circular ultra-high performance concrete specimens. *Struct. Eng. Mech.* 50 (6), 709–722. doi:10.12989/sem.2014.50.6.709

Hannawi, K., Bian, H., Prince-Agbodjan, W., and Raghavan, B. (2016). Effect of different types of fibers on the microstructure and the mechanical behavior of Ultra-High Performance Fiber-Reinforced Concretes. *Compos. Part B Eng.* 86, 214–220. doi:10.1016/j.compositesb.2015.09.059

Hoang, A. L., Fehling, E., Lai, B., Thai, D. K., and Chau, N. V. (2019). Experimental study on structural performance of UHPC and UHPFRC columns confined with steel tube. *Eng. Struct.* 187, 457–477. doi:10.1016/j.engstruct.2019.02.063

Huang, L., Xie, J., Li, L., Xu, B., Huang, P., and Lu, Z. (2021). Compressive behaviour and modelling of CFRP-confined ultra-high performance concrete under cyclic loads. *Constr. Build. Mater.* 310, 124949. doi:10.1016/j.conbuildmat.2021.124949

Lam, L., Huang, L., Xie, J.-H., and Chen, J. F. (2021). Compressive behavior of ultra-high performance concrete confined with FRP. *Compos. Struct.* 274, 114321. doi:10.1016/j.compstruct.2021.114321

Lam, L., and Teng, J. G. (2003). Design-oriented stress–strain model for FRP-confined concrete. *Constr. Build. Mater.* 17 (6–7), 471–489. doi:10.1016/s0950-0618(03)00045-x

Li, B., and Zhou, W. (2022). Experimental and finite element analysis on axial compression performance of concrete columns confined with CFRP tubes. . *Mater. Rep.* 36 (S1), 246–251.

Liang, X. Y., Chi, Y., and Zeng, Y. Q. (2020). Experimental studies on stress-strain relationship of ultra-high performance concrete confined by GFRP tube under uniaxial compression. *Eng. J. Wuhan Univ.* 53 (6), 498–506. doi:10.1016/j.engstruct.2021.113246

Liao, J., Yang, K. Y., Zeng, J.-J., Quach, W. M., Ye, Y. Y., and Zhang, L. (2021). Compressive behavior of FRP-confined ultra-high performance concrete (UHPC) in circular columns. *Eng. Struct.* 249, 113246. doi:10.1016/j.engstruct.2021.113246

Liao, J., Zeng, J.-J., Gong, Q.-M., Quach, W. M., Gao, W. Y., and Zhang, L. (2022). Design-oriented stress-strain model for FRP-confined ultra-high performance concrete (UHPC). *Constr. Build. Mater.* 318, 126200. doi:10.1016/j.conbuildmat.2021.126200

Liao, J., Zeng, J.-J., Lin, X.-C., and Zhuge, Y. (2023a). Punching shear behavior of FRP grid-reinforced ultra-high performance concrete slabs. *J. Compos. Constr.* 27 (4), 04023031. doi:10.1061/jccof2.cceng-4148

Liao, J., Zeng, J.-J., Zhuge, Y., Zheng, Y., Ma, G., and Zhang, L. (2023b). FRP-confined concrete columns with a stress reduction-recovery behavior: a state-of-the-art review, design recommendations and model assessments. *Compos. Struct.* 321, 117313. doi:10.1016/j.compstruct.2023.117313

Liu, J., Li, J., Fang, J., Su, Y., and Wu, C. (2022). Ultra-high performance concrete targets against high velocity projectile impact–a-state-of-the-art review. *Int. J. Impact Eng.* 160, 104080. doi:10.1016/j.ijimpeng.2021.104080

Lu, J. P. (2020). *Compression behavior of FRP confined ultra high performance concrete [D]*. Bangladesh: Southeast University.

Luo, M., Lin, P. Z., and Yang, Z. J. (2020). Study of mechanical properties and constitutive relations of UHPC under uniaxial compressive loading. *Bridge Constr.* 50 (5), 62–67. doi:10.3969/j.issn.1003-4722.2020.05.010

Ma, K., Ma, Y., Xing, G., and Liu, B. (2021). Behavior of ultra-high-performance concrete columns subjected to axial compressive load. *Adv. Struct. Eng.* 24 (16), 3792–3808. doi:10.1177/13694332211038440

Ma, K. Z., Han, X., and He, T. W. (2022). Investigation of FRP confined UHPC circular stub columns under axial compression. *J. Southwest Jiaot. Univ.* 2022, 1–9. doi:10.3969/j.issn.0258-2724.20220332

Mander, J. B., Priestley, M. J. N., and Park, R. (1988). Theoretical stress-strain model for confined concrete. *J. Struct. Eng.* 114 (8), 1804–1826. doi:10.1061/(asce)0733-9445(1988)114:8(1804)

Miao, K., Wei, Y., Dong, F., Zheng, K., and Wang, J. (2023). Experimental study on concrete-filled steel tube columns with inner distributed seawater and sea sand concrete-filled fiber-reinforced polymer tubes under axial compression. *Compos. Struct.* 320, 117181. doi:10.1016/j.compstruct.2023.117181

Mu, R., Chen, J., Chen, X., Diao, C., Wang, X., and Qing, L. (2023). Effect of the orientation of steel fiber on the strength of ultra-high-performance concrete (UHPC). *Constr. Build. Mater.* 406, 133431. doi:10.1016/j.conbuildmat.2023.133431

Ozbakkaloglu, T., Lim, J. C., and Vincent, T. (2013). FRP-confined concrete in circular sections: review and assessment of stress–strain models. *Eng. Struct.* 49, 1068–1088. doi:10.1016/j.engstruct.2012.06.010

Pimanmas, A., and Saleem, S. (2019). Evaluation of existing stress–strain models and modeling of PET FRP–confined concrete. *J. Mater. Civ. Eng.* 31 (12), 04019303. doi:10.1061/(asce)mt.1943-5533.0002941

Sadeghian, P., Rahai, A. R., and Ehsani, M. R. (2010). Effect of fiber orientation on compressive behavior of CFRP-confined concrete columns. *J. Reinf. Plastics Compos.* 29 (9), 1335–1346. doi:10.1177/0731684409102985

Saleem, S., Hussain, Q., and Pimanmas, A. (2017). Compressive behavior of PET FRP–confined circular, square, and rectangular concrete columns. *J. Compos. Constr.* 21 (3), 04016097. doi:10.1061/(asce)cc.1943-5614.0000754

Samaan, M., Mirmiran, A., and Shahawy, M. (1998). Model of concrete confined by fiber composites. *J. Struct. Eng.* 124 (9), 1025–1031. doi:10.1061/(asce)0733-9445(1998)124:9(1025)

Shan, L., and Zhang, L. (2019). Strength and fiber synergy effect of steel-polypropylene hybrid fibre-reinforced concrete. *IOP Conf. Ser. Earth Environ. Sci.* 304 (5), 052015. doi:10.1088/1755-1315/304/5/052015

Tbatou, T., and El Youbi, M. (2020). Dynamic and structural study of a RC building braced by FRP composite materials. *Int. Rev. Civ. Eng. (IRECE)* 11 (1), 1. doi:10.15866/irece.v11i1.16991

Teng, J. G., Jiang, T., and Lam, L. (2009). Refinement of a Design-Oriented Stress–Strain Model for FRP-Confined Concrete [J]. *Journal of Composites for Construction* 13 (4), 269–278. doi:10.1061/(ASCE)CC.1943-5614.0000012

Tian, H., Zhou, Z., Wei, Y., Wang, Y., and Lu, J. (2019b). Experimental investigation on axial compressive behavior of ultra-high performance concrete (UHPC) filled glass FRP tubes. *Constr. Build. Mater.* 225, 678–691. doi:10.1016/j.conbuildmat.2019.07.204

Tian, H. W., Zhou, Z., and Lu, J. P. (2019a). Effects of steel fiber content on axial compression performance of UHPC filled FRP tubes. *J. Southeast Univ. Nat. Sci. Ed.* 49 (3), 481–487. doi:10.3969/j.issn.1001-0505.2019.03.011

Tian, H. W., Zhou, Z., and Lu, J. P. (2020). Meso-scale numerical simulation of axial compression performance of fiber reinforced polymer composite-confined ultra-high performance concrete. *Acta Mater. Compos. Sin.* 37 (7), 1629–1638. doi:10.13801/j.cnki.fhclxb.20190827.001

Toutanji, H. A. (1999). Stress-strain characteristics of concrete columns externally confined with advanced fiber composite sheets. *ACI Struct. J.* 96 (3), 397–404.

Vincent, T., and Ozbakkaloglu, T. (2013). Influence of fiber orientation and specimen end condition on axial compressive behavior of FRP-confined concrete. *Constr. Build. Mater.* 47, 814–826. doi:10.1016/j.conbuildmat.2013.05.085

Wang, G., Wei, Y., Shen, C., Huang, Z., and Zheng, K. (2023a). Compression performance of FRP-steel composite tube-confined ultrahigh-performance concrete (UHPC) columns. *Thin-Walled Struct.* 192, 111152. doi:10.1016/j.tws.2023.111152

Wang, H. (2022). Review of research on ultra-high performance concrete. *China Concr. Cem. Prod.* (4), 25–28. doi:10.19761/j.1000-4637.2022.04.025.04

Wang, J. J., Zhang, S. S., Nie, X. F., and Yu, T. (2023b). Compressive behavior of FRP-confined ultra-high performance concrete (UHPC) and ultra-high performance fiber reinforced concrete (UHPFRC). *Compos. Struct.* 312, 116879. doi:10.1016/j.compstruct.2023.116879

Wang, W., Wu, C., Liu, Z., and Si, H. (2018b). Compressive behavior of ultra-high performance fiber-reinforced concrete (UHPFRC) confined with FRP. *Compos. Struct.* 204, 419–437. doi:10.1016/j.compstruct.2018.07.102

Wang, Y., Feng, J., and Li, J. Y. (2018a). Advance of FRP anchor bolts in geotechnical anchoring. *J. Eng. Geol.* 26 (3), 776–784. doi:10.13544/j.cnki.jeg.2017-139

Wang, Y., Liu, P., Cao, Q., Chen, G., Wan, B., Wei, Z., et al. (2021). Comparison of monotonic axial compressive behavior of rectangular concrete confined by FRP with different rupture strains. *Constr. Build. Mater.* 299, 124241. doi:10.1016/j.conbuildmat.2021.124241

Wu, G., Lv, Z. T., and Wu, Z. S. (2006). Strength and ductility of concrete cylinders confined with FRP composites. *Constr. Build. Mater.* 20, 134–148. doi:10.1016/j.conbuildmat.2005.01.022

Wu, Z., Shi, C., He, W., and Wu, L. (2016). Effects of steel fiber content and shape on mechanical properties of ultra high performance concrete. *Constr. Build. Mater.* 103, 8–14. doi:10.1016/j.conbuildmat.2015.11.028

Xu, L., Lu, Q., Chi, Y., Yang, Y., Yu, M., and Yan, Y. (2019). Axial compressive performance of UHPC filled steel tube stub columns containing steel-polypropylene hybrid fiber. *Constr. Build. Mater.* 204, 754–767. doi:10.1016/j.conbuildmat.2019.01.202

Yağar, A. C., İnce, C., and Derogar, S. (2022). FRP strengthening of RC structures: sustainable, environmental and structural evaluations. *J. Sustain. Constr. Mater. Technol.* 7 (4), 358–374. doi:10.47481/jscmt.1211086

Yoo, D.-Y., Banthia, N., Kang, S.-T., and Yoon, Y. S. (2016). Size effect in ultra-high-performance concrete beams. *Eng. Fract. Mech.* 157, 86–106. doi:10.1016/j.engfracmech.2016.02.009

Yoo, D.-Y., Lee, J.-H., and Yoon, Y.-S. (2013). Effect of fiber content on mechanical and fracture properties of ultra high performance fiber reinforced cementitious composites. *Compos. Struct.* 106, 742–753. doi:10.1016/j.compstruct.2013.07.033

Yu, K.-Q., Yu, J.-T., Dai, J.-G., Lu, Z. D., and Shah, S. P. (2018). Development of ultra-high performance engineered cementitious composites using polyethylene (PE) fibers. *Constr. Build. Mater.* 158, 217–227. doi:10.1016/j.conbuildmat.2017.10.040

Yuan, W.-Y., Han, Q., and Bai, Y.-L. (2022b). A unified stress-strain model for LRS FRP-confined concrete columns with square and circular cross-sections. *Eng. Struct.* 255, 113900. doi:10.1016/j.engstruct.2022.113900

Yuan, W. Y., Han, Q., and Bai, Y. L. (2022a). A unified confinement model of FRP-wrapped concrete cylinder. *China J. Highw. Transp.* 35 (2), 146–158. doi:10.19721/j.cnki.1001-7372.2022.02.013

Zeng, J.-J., Ye, Y.-Y., Gao, W.-Y., Smith, S. T., and Guo, Y. C. (2020). Stress-strain behavior of polyethylene terephthalate fiber-reinforced polymer-confined normal-high- and ultra high-strength concrete. *J. Build. Eng.* 30, 101243. doi:10.1016/j.jobe.2020.101243

Zeng, L., Yu, W., Mo, Z., Huang, S. q., and Yuan, H. (2023). Experimental and numerical studies on sea sand concrete filled stainless steel tube with inner FRP tube subjected to axial compression. *China Ocean. Eng.* 37 (2), 272–287. doi:10.1007/s13344-023-0023-5

Zhang, B., Wei, W., and Feng, G. S. (2019). Influences of fiber angles on axial compressive behavior of GFRP-confined concrete stub column. *J. Build. Struct.* 40 (S1), 192–199. doi:10.14006/j.jzjgxb.2019.S1.025

Zhang, S. S., Wang, J. J., Lin, G., Yu, T., and Fernando, D. (2023b). Stress-strain models for ultra-high performance concrete (UHPC) and ultra-high performance fiber-reinforced concrete (UHPFRC) under triaxial compression. *Constr. Build. Mater.* 370, 130658. doi:10.1016/j.conbuildmat.2023.130658

Zhang, X., Wang, H., Zhang, Y., and Wang, L. (2023a). Corrosion of steel rebars across UHPC joint interface under chloride attack. *Constr. Build. Mater.* 387, 131591. doi:10.1016/j.conbuildmat.2023.131591

Zhao, P., Huang, Y., Liu, Z., Lu, Y., and Wang, H. (2022a). Experimental study on seismic performance of hybrid steel-polypropylene fiber-reinforced recycled aggregate concrete-filled circular steel tube columns. *Constr. Build. Mater.* 359, 129418. doi:10.1016/j.conbuildmat.2022.129418

Zhao, Y., Cao, X., and Chen, C. C. (2022b). Effect of steel fiber on properties of ultra-high performance concrete. *Jiangsu Build. Mater.* (6), 11–13. doi:10.3969/j.issn.1004-5538.2022.06.005

Zhao, Z., Wei, Y., Wang, G., Miao, K., and Zheng, K. (2023b). Exploration on unified calculation of axial compressive load-carrying capacity of square and rectangular concrete-filled steel tubular columns. *Constr. Build. Mater.* 398, 132546. doi:10.1016/j.conbuildmat.2023.132546

Zhao, Z., Wei, Y., Wang, G., Zhang, Y., and Lin, Y. (2023a). Axial compression performance of square UHPC-filled stainless-steel tubular columns. *Constr. Build. Mater.* 408, 133622. doi:10.1016/j.conbuildmat.2023.133622

Zhu, M. Q., Tan, X. P., and Liu, W. L. (2023). Pseudostatic experimental study of GFRP tube constraining UHPC column. *J. Hunan Univ. Sci. Technol. Nat. Sci. Ed.* 38 (1), 25–34. doi:10.13582/j.cnki.1672-9102.2023.01.004

Zohrevand, P., and Mirmiran, A. (2011). Behavior of ultrahigh-performance concrete confined by fiber-reinforced polymers. *J. Mater. Civ. Eng.* 23 (12), 1727–1734. doi:10.1061/(asce)mt.1943-5533.0000324

Zohrevand, P., and Mirmiran, A. (2013). Stress-strain model of ultrahigh performance concrete confined by fiber-reinforced polymers. *J. Mater. Civ. Eng.* 25 (12), 1822–1829. doi:10.1061/(asce)mt.1943-5533.0000769